



Article

Synthesis, Characterization, and Crystal Structure Determination of a New Lithium Zinc Iodate Polymorph $\text{LiZn}(\text{IO}_3)_3$

Zoulikha Hebboul ¹, Christine Galez ², Djamal Benbortal ¹, Sandrine Beauquis ², Yannick Mugnier ² , Abdelnour Benmakhlouf ³, Mohamed Bouchenafa ⁴ and Daniel Errandonea ^{5,*} 

¹ Laboratoire Physico-Chimie des Matériaux (LPCM), University Amar Telidji of Laghouat, BP 37G, Ghardaïa Road, Laghouat 03000, Algeria

² Univ. Savoie Mont Blanc, SYMME, F-74000 Annecy, France

³ Laboratoire de Caractérisation et Valorisation des Ressources Naturelles, Université de Bordj Bou-Arreidj, El-Anasser 34030, Algeria

⁴ Fundamental and Applied Physics Laboratory-Physics Department, University of Blida 1, route de Soumaa BP 270, Blida 09000, Algeria

⁵ Departamento de Física Aplicada-ICMUV-MALTA Consolider Team, Universitat de València, c/Dr. Moliner 50, 46100 Burjassot (Valencia), Spain

* Correspondence: daniel.errandonea@uv.es

Received: 5 August 2019; Accepted: 1 September 2019; Published: 4 September 2019



Abstract: Synthesis and characterization of anhydrous $\text{LiZn}(\text{IO}_3)_3$ powders prepared from an aqueous solution are reported. Morphological and compositional analyses were carried out by using scanning electron microscopy and energy-dispersive X-ray measurements. The synthesized powders exhibited a needle-like morphology after annealing at 400 °C. A crystal structure for the synthesized compound was proposed from powder X-ray diffraction and density-functional theory calculations. Rietveld refinements led to a monoclinic structure, which can be described with space group $P2_1$, number 4, and unit-cell parameters $a = 21.874(9)$ Å, $b = 5.171(2)$ Å, $c = 5.433(2)$ Å, and $\beta = 120.93(4)^\circ$. Density-functional theory calculations supported the same crystal structure. Infrared spectra were also collected, and the vibrations associated with the different modes were discussed. The non-centrosymmetric space group determined for this new polymorph of $\text{LiZn}(\text{IO}_3)_3$, the characteristics of its infrared absorption spectrum, and the observed second-harmonic generation suggest it is a promising infrared non-linear optical material.

Keywords: iodate; crystal structure; X-ray diffraction; density functional theory; infrared absorption

1. Introduction

Metal iodates form a series of compounds potentially useful as dielectric materials and in non-linear optics [1–4]. They can also be employed for other applications like desalination and water treatment [5]. Among them, alkali metal iodates [6], $\alpha\text{-HIO}_3$ [7], and ammonium iodate [8] have attracted large attention not only because of their non-linear optical properties but also because of their piezoelectric and pyroelectric responses. For instance, lithium iodate (LiIO_3) has been widely used as a piezoelectric, acousto-optic, and second-harmonic generation (SHG) material [9]. However, LiIO_3 crystals occasionally have OH inclusions which reduce their transparency in the infrared (IR) region, affecting their performance [10]. In addition, their properties are known to strongly depend on the growth conditions [11]. Transition metal iodates free of OH inclusions, e.g., $\text{Zn}(\text{IO}_3)_2$, have thus been developed as alternative materials with high SHG efficiency [12]. It is generally accepted that the important electro

and nonlinear optical properties of metal iodates originate from the lone electron pair of iodine in the IO_3^- iodate anion [13]. A lot of efforts have thus been dedicated to the synthesis of compounds containing this anion [14–19]. Iodates which combine two types of cations also constitute a particularly interesting group. For instance, attention has been devoted to the synthesis of double iodates like $\text{LiFe}_{1/3}(\text{IO}_3)_2$ [20], which exhibit higher nonlinear coefficients than LiIO_3 and transition metal iodates [21]. Solid-solution $\text{Li}_x\text{Fe}_{1-x}\text{Zn}_x(\text{IO}_3)_3$ crystals have been also studied [22]. Among the double iodates, another material of special significance is $\text{LiZn}(\text{IO}_3)_3$, prepared in the past by solid-state sintering [23] and reported to be an excellent ionic conductor and to have a remarkable SHG. An orthorhombic structure was then proposed, but the space group and atomic positions were not determined [23]. We report here on a facile, cheap, and environmentally friendly synthesis route for anhydrous $\text{LiZn}(\text{IO}_3)_3$. A possible crystal structure is proposed based upon powder X-ray diffraction (XRD) experiments and Rietveld refinements. The structural determination is also supported by density-functional theory (DFT) calculations. Details of the morphology and IR spectral properties of the compound are also presented.

2. Materials and Methods

2.1. Sample Preparation

The compound was synthesized from an aqueous solution of LiIO_3 (Sigma-Aldrich 99%, St. Louis, MO, USA) and ZnCl_2 (Riedel-de Haën 98%, Hannover, Lower Saxony, Germany). Lithium iodate was first dissolved into 65% concentrated nitric acid obtained from Merck (4 mmol of LiIO_3 in 10 ml of 16N nitric acid) and then added to an anhydrous zinc chloride solution (1 mmol in 10 ml of 16N nitric acid). After being stirred thoroughly, the reaction mixture was slowly evaporated and maintained at 55 °C for four days, leading to the formation of an amorphous white precipitate. After filtration and washing with de-ionized water, the product was finally heat-treated at 400 °C for two hours in a tubular furnace.

2.2. Sample Characterization

The synthesized powders were analyzed under scanning electron microscopy (SEM), powder X-ray diffraction (XRD), and Fourier transform infrared spectroscopy (FTIR). Phase purity and crystal structure of $\text{LiZn}(\text{IO}_3)_3$ crystals were evaluated by XRD using a Philips-Xpert pro diffractometer (Amsterdam, North Holland, Netherlands) using $\text{Cu K}\alpha_1$ ($\lambda = 1.54056 \text{ \AA}$) and $\text{K}\alpha_2$ ($\lambda = 1.54443 \text{ \AA}$) radiation ($\text{K}\alpha_2/\text{K}\alpha_1$ ratio = 0.5), with a step size of $2\theta = 0.02^\circ$ and sweeping with a 0.2° per minute velocity. The structural analysis was carried out using Powdercell [24] and FullProf [25]. For the structural refinement, the background was fitted with a six-order polynomial function, and the peak profiles were modelled using a pseudo-Voigt function [26], using the Caglioti formula [27] for the angular dependence of the full-width at half-maximum of the Bragg peaks. On the other hand, the refinement did not include the isotropic displacement factors which were assumed to be 1.0 \AA^2 , a typical value for lithium oxides and iodates [28–30], but included an overall displacement factor (B) [31]. Homogeneity and partial chemical composition of the samples were first assessed by SEM (VEGA\TESCAN, Brno, South Moravian Region, Czech Republic) with a Peltier cooled XFlashTM silicon drift detector (model 410 M) for energy-dispersive X-ray (EDX) analysis. Secondary electron images were recorded using 20 keV primary electrons. FTIR spectra (Jasco FT/IR-4200 instrument, Halifax, NS, Canada) were acquired after dispersing the $\text{LiZn}(\text{IO}_3)_3$ powder on a KBr carrier, and a strong naked-eye SHG signal was observed from a collimated, pulsed 1064 nm excitation laser (Wedge HB, Bright solutions, pulse width 1 ns, repetition rate 1 kHz, Cura Carpignano, Pavia, Italy).

2.3. Density-Functional Theory Calculations

Density-functional theory (DFT) is a quantum mechanics calculation method that gives an accurate description of the structural and physical properties of different compounds, in particular, oxides [32]. Accuracy of the results previously obtained by using DFT on different oxides [31,33], including LiIO_3 [34], supports its application in the case of $\text{LiZn}(\text{IO}_3)_3$. The total-energy DFT simulations reported here

were performed at zero temperature, by using the ab initio plane-wave pseudopotential total-energy calculations as implemented in the CASTEP code [35]. This code has the advantage that partial atom occupancies (as in the compound studied) can be easily implemented by constructing a supercell ($4 \times 4 \times 4$) of the studied material, containing vacancies to get a composition consistent with the required stoichiometry. In the calculations, the exchange correlation energy was described in the general-gradient approximation (GGA) using the Perdew–Wang 1991 (PW91) pseudopotentials [36] with a kinetic cut-off energy of 500 eV for the plane-wave expansions. The reciprocal space integration was performed using $4 \times 4 \times 4$ k-point grids in the Brillouin zone, and the geometry optimization used the Broyden–Fletcher–Goldfarb–Shannon (BFGS) algorithm. The lattice parameters and atomic positions were fully optimized through the minimization of the total energy and forces on atoms. Finally, the total energy was converged for an accuracy of 1 meV/atom, and the Hellmann–Feynmann forces on each atom were converged to less than 0.01 eV/Å.

3. Results and Discussion

3.1. Morphology and Composition

Energy-dispersive X-ray spectroscopy (EDX) was used to confirm the composition and phase purity of the prepared $\text{LiZn}(\text{IO}_3)_3$ samples. Within the limits of experimental error, EDX analyses by both weight percent and atomic percent of Zn and I were found to be in agreement with their corresponding expected molar ratio of 1:3. The measured Zn and I contents were 24.9(5) at% and 75.1(5) at%, respectively. The content of Zn and I was determined using the ESPRIT Microanalysis Software from Bruker (Billerica, MA, USA). The presence of impurities was not detectable within the resolution of the instrument.

Figure 1 shows the morphology and size of the synthesized material. As clearly evidenced from the scanning electron microscopy (SEM) micrograph, the $\text{LiZn}(\text{IO}_3)_3$ powder is constituted of micron sized needle-like particles. Their length varies between 10 and 100 μm , and their diameter is smaller than 2 μm .

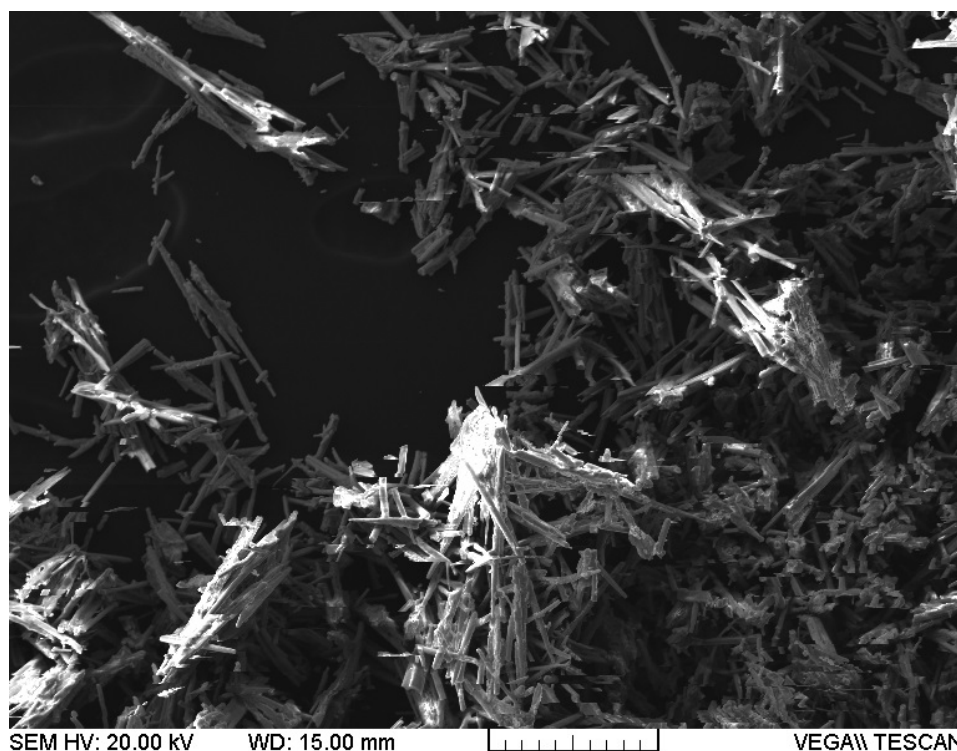


Figure 1. SEM morphology of the $\text{LiZn}(\text{IO}_3)_3$ powder. The ruler in the bottom part corresponds to 100 μm (10 $\mu\text{m}/\text{div}$).

3.2. Crystal Structure

Figure 2 shows a powder XRD pattern of $\text{LiZn}(\text{IO}_3)_3$, measured at room temperature. To obtain a phase-pure sample with a stoichiometric composition, we found that the initial Li/Zn molar ratio had to be increased to above 4:1, as stated in the sample preparation section. An excess of Li is indeed necessary to prevent the formation of $\text{Zn}(\text{IO}_3)_2$, which is otherwise obtained when the Li/Zn ratio is below 2:1. It is also well noted that washing with water is required before annealing to remove any traces of the hygroscopic $\alpha\text{-LiIO}_3$ that is also present after the evaporation step. A homogeneous and single-phase material is then readily obtained and differs from the well-known $\text{Zn}(\text{IO}_3)_2$, $\text{ZnIO}_3(\text{OH})$, and $\alpha\text{-LiIO}_3$ compounds [11,28,29,37]. As for EDX measurements, phase impurities were not detected by XRD.

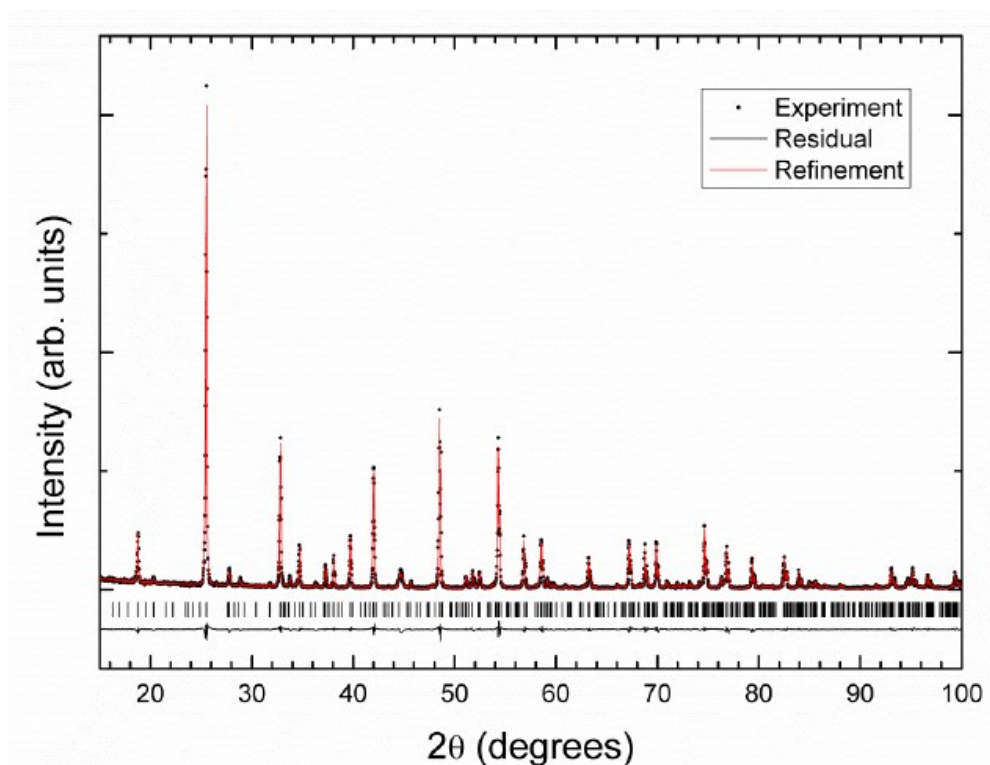


Figure 2. XRD pattern of $\text{LiZn}(\text{IO}_3)_3$ measured using $\text{Cu K}\alpha_1$ ($\lambda = 1.54056 \text{ \AA}$) and $\text{K}\alpha_2$ ($\lambda = 1.54443 \text{ \AA}$) radiation. Dots correspond to the experiment. The Rietveld refinements, carried out assuming DFT-calculated atomic positions, are shown with a red solid line. The residuals are plotted with a black solid line. Positions of the Bragg peaks are indicated by black ticks.

When analyzing the experimental XRD pattern, we found that it could not be indexed with the orthorhombic crystal structure previously reported by Sheng et al. [23]. By using the DICVOL routine, included in the FullProf Suite [25], we indexed the XRD pattern and found that the highest figure of merit corresponded to a monoclinic unit cell with parameters $a = 21.747(9) \text{ \AA}$, $b = 5.201(2) \text{ \AA}$, $c = 5.435(2) \text{ \AA}$, and $\beta = 120.28(4)^\circ$. The analysis of the systematic extinctions ($0k0$ reflections with k odd were absent) indicated $P2_1$ as the possible space group. This space group type is the same as that of the crystal structures of $\text{Zn}(\text{IO}_3)_2$ [27] and $\text{Zn}_2(\text{IO}_3)_4$ [28] (files number 54086 and number 415821 of the Inorganic Crystal Structure Database, ICSD), whereas $\text{ZnIO}_3(\text{OH})$ belongs to the monoclinic space group Cc [36], number 9 (file number 185598 of ICSD). In addition, in the case of $\text{Zn}(\text{IO}_3)_2$, the unit-cell parameters $b = 5.1158 \text{ \AA}$, $c = 5.469 \text{ \AA}$, and $\beta = 120^\circ$, are comparable with the lattice parameters b , c , and β we determined from our indexation of $\text{LiZn}(\text{IO}_3)_3$. The parameter $a = 10.938 \text{ \AA}$ of $\text{Zn}(\text{IO}_3)_2$ is, however, approximately half the parameter a we obtained for $\text{LiZn}(\text{IO}_3)_3$.

Based upon the similarities between the crystal structure of $\text{LiZn}(\text{IO}_3)_3$ and $\text{Zn}(\text{IO}_3)_2$, we built a structural model for $\text{LiZn}(\text{IO}_3)_3$ by doubling the unit-cell of $\text{Zn}(\text{IO}_3)_2$ using the group–subgroup transformation tool available in PowderCell [24]. We then assumed that Li and Zn ions alternatively occupy the positions generated from the original Zn positions and that I and O ions keep the same positions as in the original structure but with an occupation factor of 0.75 (to be consistent with the compound stoichiometry). Starting from this model, we have carried out a Rietveld refinement [37] and found that only the unit-cell parameters as well as the Li and Zn positions could be accurately determined in this way. In contrast, in the refinement, positions of the I and O atoms had to be fixed to the values obtained by doubling the unit-cell of $\text{Zn}(\text{IO}_3)_2$. This refinement procedure led otherwise to nonphysical results with some I–O bond distances too short and a reduced χ^2 smaller than 1. In order to optimize the above crystal structure determination, we also performed DFT calculations [38]. By considering the above-described structural model as the starting structure (with space group $P2_1$), we calculated the unit-cell parameters and atomic positions of all atoms for $\text{LiZn}(\text{IO}_3)_3$ by minimizing the total energy. The obtained atomic positions are summarized in Table 1. The DFT calculated unit-cell parameters were $a = 21.945 \text{ \AA}$, $b = 5.048 \text{ \AA}$, $c = 5.487 \text{ \AA}$, and $\beta = 121.07^\circ$ and agreed within 1% with those previously obtained after the refinement of the XRD pattern. Consistency between the results derived from XRD experiments and DFT calculations thus gave reliability to the proposed structural model of $\text{LiZn}(\text{IO}_3)_3$.

Table 1. Atomic positions calculated for the monoclinic $\text{LiZn}(\text{IO}_3)_3$ in the $P2_1$ space group. The table also includes the assumed occupations.

Atom	Wyckoff Position	x	y	z	Occupation
Li	2a	0.13073	0.93865	0.02872	1
Zn	2a	0.62218	0.91685	0.00530	1
I ₁	2a	0.03618	0.97718	0.33248	0.75
I ₂	2a	0.53645	0.95209	0.33300	0.75
I ₃	2a	0.30300	0.97387	0.33483	0.75
I ₄	2a	0.79086	0.98644	0.32689	0.75
O ₁	2a	0.45968	0.17690	0.33564	0.75
O ₂	2a	0.95849	0.20846	0.28041	0.75
O ₃	2a	0.10713	0.16625	0.67254	0.75
O ₄	2a	0.60797	0.15273	0.65619	0.75
O ₅	2a	0.05892	0.18401	0.08682	0.75
O ₆	2a	0.54373	0.16225	0.03871	0.75
O ₇	2a	0.38252	0.19763	0.66145	0.75
O ₈	2a	0.86320	0.20816	0.63333	0.75
O ₉	2a	0.22246	0.15968	0.31462	0.75
O ₁₀	2a	0.70911	0.14574	0.29944	0.75
O ₁₁	2a	0.30225	0.17019	0.03227	0.75
O ₁₂	2a	0.78937	0.19692	0.01147	0.75

To go further, we then performed additional Rietveld refinements by using a different strategy, namely, the atomic positions obtained from DFT calculations were fixed in the structural model. The occupancies were also constrained to the values given in Table 1. The remaining parameters such as: unit-cell parameters (obtained values given below), peak-shape parameters ($u = 0.0085$, $v = 0.059$, $w = 0.084$), isotropic displacement factor ($B = 2.34$), and scale factor (1.15) were then all refined similarly to previous studies where the atomic positions of oxygen atoms were hardly determined without a similar approach [39,40]. The structural model given in Table 1 finally led to the smallest residuals (the R-factors were $R_p = 2.36\%$ and $R_{wp} = 3.18\%$, and a reduced χ^2 was equal to 1.145) and a good-quality fit, as illustrated in Figure 2. The unit-cell parameters obtained after the new Rietveld refinement, based on calculated atomic positions, were $a = 21.874(9) \text{ \AA}$, $b = 5.171(2) \text{ \AA}$, $c = 5.433(2) \text{ \AA}$, and $\beta = 120.93(4)^\circ$, with a fit accuracy that supported the assignment of the proposed monoclinic structure to the space group $P2_1$ [41,42]. It is also important to highlight here that the unit-cell volume

(527.04 Å³) of LiZn(IO₃)₃, which had a molar mass of 597.03 g/mol and two formula units per cell ($Z = 2$), was slightly smaller than twice the unit-cell volume of Zn(IO₃)₂ (265.02 Å³). This could be a consequence of the partial occupation of the atomic sites of the iodine and oxygen atoms. Finally, as in other iodates, the determination of the exact position of the light Li atoms would deserve complementary neutron diffraction experiments [43].

The as-obtained crystal structure of LiZn(IO₃)₃ is shown in Figure 3. In Table 2, we report the different interatomic bond distances. A structural comparison with the structures of Zn(IO₃)₃ and α -LiIO₃ [11,27] showed that there are many similarities regarding polyhedral units and connectivities. In particular, the structure of the monoclinic polymorph of LiZn(IO₃)₃ can be described as a three-dimensional network of molecular ZnO₆ and LiO₆ octahedral units that are solely connected by monodentate iodate groups which have an asymmetric coordination. The main difference between LiZn(IO₃)₃ and the other compounds is the missing of $\frac{1}{4}$ of the iodate groups. The IO₃ polyhedron exhibited the expected trigonal-pyramidal configuration with three different short I–O bond distances, which slightly changed from one IO₃ polyhedron to another, as can be seen in Table 2. These distances ranged from 1.9037(5) to 2.0833(5) Å. Each iodine atom had three additional oxygen neighbors, which were on the side of the lone-pair electrons of iodide. These weakly linked oxygen atoms were at longer distances, with interatomic distances going from 2.1952(5) to 2.7772(5) Å, thus forming a highly distorted IO₆ polyhedron. The ZnO₆ and LiO₆ octahedral units were slightly distorted, with an average bond length of 2.168(3) and 2.155(3) Å, respectively. The quadratic elongation for the ZnO₆ (LiO₆) octahedron was 1.0064 (1.0052), and the distortion index was 0.01358 (0.01699). These two parameters, that are commonly used to describe distortions within a coordination octahedron, were calculated using VESTA [44] according to the definitions given by Robinson and Bauer [45].

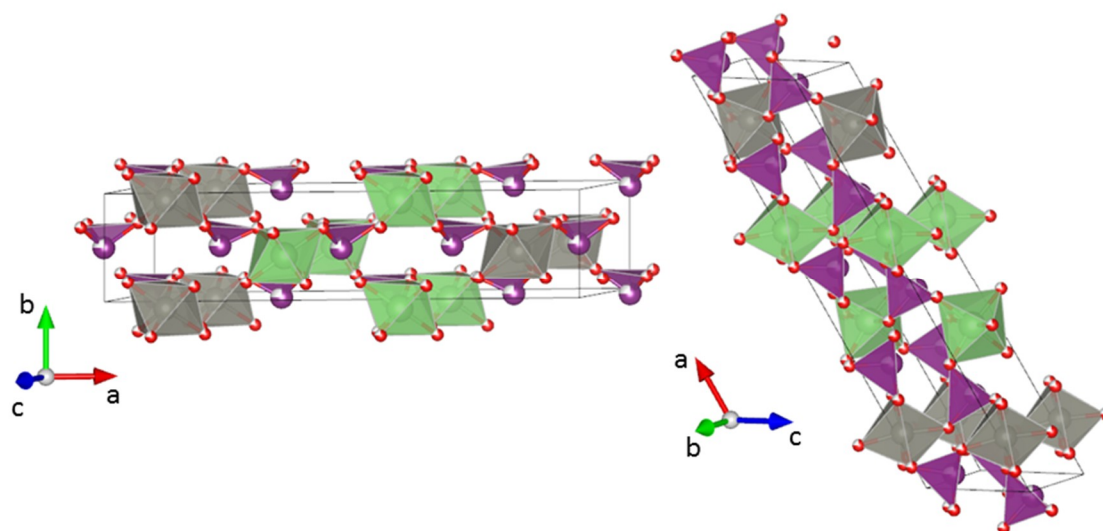


Figure 3. Schematic view of the crystal structure of LiZn(IO₃)₃. Zn (Li) atoms are shown in gray (green), I atoms in violet, and O atoms in red. The site occupation of the last two types of atoms is 0.75. The different coordination polyhedra are shown.

We would like to comment on the fact that the monoclinic structure reported here is different from the orthorhombic structure previously reported [23]. One possibility is that diverse polymorphs were obtained because of the different chemical routes used in the synthesis (starting reagents, solvent, temperature, crystallization pathways, etc.). For instance, in lithium iodate, the processing parameters have a key influence on the three different crystalline structures that can be stabilized at room temperature [46]. A second option, which should not be excluded, is the incorrect assignment of the crystal structure in the previous study [23]. Previously, only the unit-cell parameters were specified, but not the space group and atomic positions. The authors reported that the unit-cell

corresponds to four formula units, which implies a volume per formula unit 25% smaller than in $\text{Zn}(\text{IO}_3)_3$ and LiIO_3 , which is unexpected, since $\text{ZnLi}(\text{IO}_3)_3$ is a binary solution of these. In contrast, as we described above, the monoclinic structure here proposed has many similarities with the structures of $\text{Zn}(\text{IO}_3)_2$ and $\alpha\text{-LiIO}_3$. This and the consistency of DFT calculations further support the crystal structure here reported.

Table 2. Zn–O, Li–O, and I–O interatomic distances in the different coordination polyhedra of $\text{LiZn}(\text{IO}_3)_3$.

Bond	Distance	Bond	Distance	Bond	Distance
Zn–O	2.1087(5) Å	I ₁ –O	1.9571(5) Å	I ₃ –O	1.9249(5) Å
	2.1391(5) Å		1.9634(5) Å		1.9596(5) Å
	2.1789(5) Å		1.9758(5) Å		2.0833(5) Å
	2.1828(5) Å		2.4729(5) Å		2.4011(5) Å
	2.1834(0) Å		2.5285(5) Å		2.5406(5) Å
	2.2154(0) Å		2.6350(5) Å		2.7273(5) Å
Li–O	2.0903(5) Å	I ₂ –O	1.9450(5) Å	I ₄ –O	1.9037(5) Å
	2.1310(5) Å		2.0061(5) Å		1.9702(5) Å
	2.1351(5) Å		2.0484(5) Å		2.0161(5) Å
	2.1626(5) Å		2.1952(5) Å		2.5582(5) Å
	2.1648(5) Å		2.2619(5) Å		2.7049(5) Å
	2.2487(5) Å		2.3999(5) Å		2.7772(5) Å

In terms of functional properties, it is worth mentioning that the new polymorph of $\text{LiZn}(\text{IO}_3)_3$ crystallized in a polar space group ($P2_1$) and is therefore a potential material for SHG with similar functionalities as LiIO_3 and $\text{Zn}(\text{IO}_3)_2$ [47]. The $P2_1$ space group belongs to class 2 for which eight (respectively 4) nonzero SHG coefficients are to be considered without (respectively with) Kleinman's symmetry. So far, an accurate assessment of the independent SHG coefficients and overall conversion efficiency could not be obtained because of the needle-like morphology. However, a bright green spot was observed under a 1064 nm laser excitation on powder agglomerates, suggesting that the produced SHG signal was very strong. Another interesting specificity of $\text{LiZn}(\text{IO}_3)_3$, arising from its crystal structure, is the number of vacant sites and the zig-zag polyhedral chains running parallel to the *a*-axis (see Figure 3). Li^+ ionic conductivity [48,49] as well as highly anisotropic compression and thermal expansion are thus expected [50]. Other properties such as the bulk modulus could be estimated from empirical relations, assuming that compression is dominated by the ZnO_6 and LiO_6 octahedral units, from the Zn–O and Li–O bond distances and the formal charge of Zn and Li [51]. The obtained value was 55 GPa. It agrees with the measured bulk modulus of $\alpha\text{-LiIO}_3$ [52], being therefore a plausible estimation of the bulk modulus of $\text{LiZn}(\text{IO}_3)_3$.

3.3. FTIR Spectroscopy

Results of the Fourier transform infrared spectroscopy (FTIR) measurements will be next discussed. Figure 4 shows the transmission spectrum in the 4000–400 cm^{-1} region, with a zoom in the 900–500 cm^{-1} region. The zoom is shown in the inset to facilitate the identification of modes associated with the iodate anion. In the FTIR spectrum, we have automatically subtracted the CO_2 bands from atmosphere absorption, although weak artifacts originated by CO_2 are still present in the corrected data around 2300 cm^{-1} . According to group theory, $\text{LiZn}(\text{IO}_3)_3$ has 81 IR-active modes ($\Gamma = 41\text{A} + 40\text{B}$), which is considerably more than the 51 IR-active modes ($\Gamma = 26\text{A} + 25\text{B}$) of $\text{Zn}(\text{IO}_3)_2$. This led to a broadening of the IR bands of $\text{LiZn}(\text{IO}_3)_3$ due to partial phonon overlaps.

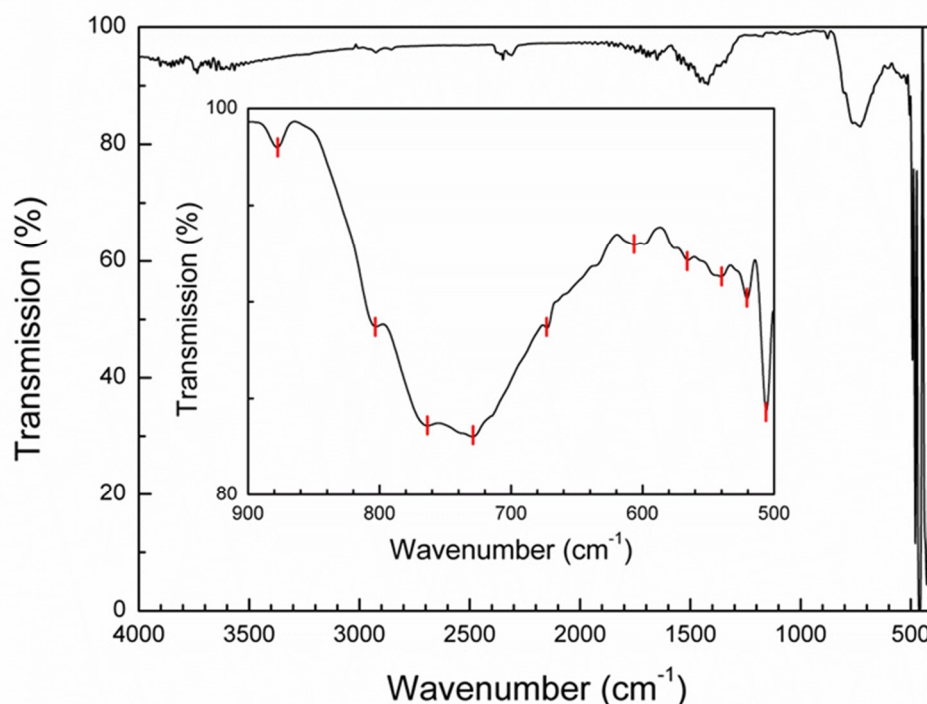


Figure 4. FTIR spectrum of $\text{LiZn}(\text{IO}_3)_3$ in the $4000\text{--}400\text{ cm}^{-1}$ region. The inset shows a zoom in the $900\text{--}500\text{ cm}^{-1}$ range. Ticks indicate position of the absorption peaks listed in the text.

A better near-infrared transparency of $\text{LiZn}(\text{IO}_3)_3$, as compared to $\alpha\text{-LiIO}_3$, could be noticed [53]. In addition, the spectral frequency range at $4000\text{--}3200\text{ cm}^{-1}$ is very useful to witness the presence of OH groups [54]. Here, a very low content of residual OH bonds was observed, in agreement with the acidic synthesis conditions used for the preparation of $\text{LiZn}(\text{IO}_3)_3$. On the other hand, substitution of Li^+ by H^+ ions was very unlikely, since the specific O-H \cdots O vibrations of similar intensity observed at about 590 and 730 cm^{-1} in $\text{Li}_{1-x}\text{H}_x(\text{IO}_3)$ [55] were not detected here. The band located from 1900 cm^{-1} to 1250 cm^{-1} could correspond to the second overtone of phonons from the $900\text{--}600\text{ cm}^{-1}$ band [56] or to the presence of H_2O molecules [57], which is less probable after crystallization annealing at 400°C . Between 900 and 600 cm^{-1} , several absorption features at 607 , 673 , 729 , 764 , 803 , and 877 cm^{-1} were noticed and denoted by ticks in the inset of Figure 4. Additional absorption peaks below 600 cm^{-1} could also be seen at 506 , 521 , 540 , and 566 cm^{-1} .

Regarding the assignment of the iodate IR modes, we first considered that the vibrational frequencies of the symmetrical pyramidal IO_3^- ion in solutions and compounds are ν_1 (symmetric stretching) at $780\text{--}630\text{ cm}^{-1}$, ν_2 (symmetric bending) at about $400\text{--}350\text{ cm}^{-1}$, ν_3 (asymmetric stretching) at $820\text{--}730\text{ cm}^{-1}$, and ν_4 (asymmetric bending) at about 330 cm^{-1} [54,56,57]. The presence of the distorted IO_6 polyhedral units, as evidenced by XRD, was expected to induce noticeable changes in the IR absorption spectrum of $\text{LiZn}(\text{IO}_3)_3$ compared to simple metal iodates. Two additional frequencies could be foreseen, since degeneracy of the two asymmetric fundamental vibrations ν_3 and ν_4 was no longer present [54]. By analogy with other iodates, the five absorption peaks observed between 900 and 630 cm^{-1} could be assigned to the I–O stretching vibrations of the IO_3 polyhedron, but the occurrence in the $\text{LiZn}(\text{IO}_3)_3$ structure of pyramidal IO_3^- ions and of IO_6 octahedral units made the IR spectra more complicated [12]. It was therefore difficult to assign the bands unambiguously, especially as the pyramidal and octahedral geometries were distorted. Finally, the absorption bands occurring between 673 and 500 cm^{-1} could be ascribed to the first overtones of the iodate ion bending modes, with some lattice mode contributions involving vibrations between metal ions and IO_3 as a rigid unit.

4. Conclusions

A new polymorph of $\text{LiZn}(\text{IO}_3)_3$ was synthesized by a simple low-cost co-precipitation route and heat-treatment of the amorphous precipitate at 400 °C. The combination of Rietveld refinements of the powder XRD pattern and DFT calculations resulted in a monoclinic crystalline lattice with the non-centrosymmetric space group $P2_1$. The unit-cell parameters and atomic positions were also determined. We also performed EDX and SEM measurements that confirmed the phase purity and demonstrated that the synthesized $\text{LiZn}(\text{IO}_3)_3$ had a needle-like morphology. Finally, a FTIR analysis further supported the preparation of phase-pure $\text{LiZn}(\text{IO}_3)_3$ without the occurrence of H^+ ions. Because of the low symmetry of point group 2, a detailed assignment of each IR experimental frequency was not conducted, but FTIR measurements were found consistent with those of other iodate compounds. More importantly, because of its non-centrosymmetric polar crystal structure, as well as its wide transparency and chemical stability compared to the very hygroscopic $\alpha\text{-LiIO}_3$, $\text{LiZn}(\text{IO}_3)_3$ appears as a good candidate for non-linear optical applications. Besides, nanocrystal suspensions are under preparation so as to quantitatively assess, in the near future, the averaged SHG coefficients, as already reported for other oxide nanomaterials [58].

Author Contributions: Conceptualization, Z.H., C.G., Y.M. and D.E.; Formal analysis, Z.H., C.G., D.B., S.B., Y.M. and D.E.; Investigation, Z.H., C.G., D.B., S.B. and Y.M.; Computer simulations, A.B. and M.B.; Writing—Review and Editing, Z.H., Y.M. and D.E.

Funding: This work was supported by the Spanish Ministry of Science, Innovation and Universities under grant MAT2016-75586-C4-1-P and by Generalitat Valenciana under grant Prometeo/2018/123 (EFIMAT). Y.M., S.B., and C.G. gratefully acknowledge support from the French-Swiss Interreg Program (NANOFIMT project).

Conflicts of Interest: The authors declare no conflict of interest.

References

- Guo, S.P.; Chi, Y.; Guo, G.C. Recent achievements on middle and far-infrared second-order nonlinear optical materials. *Coord. Chem. Rev.* **2017**, *335*, 44–57. [\[CrossRef\]](#)
- Xiao, L.; Zhenbo, Y.; Yao, J.Y.; Lin, Z.S.; Hu, Z.G. A new cerium iodate infrared nonlinear optical material with a large second-harmonic generation response. *J. Mater. Chem. C* **2017**, *5*, 2130–2134. [\[CrossRef\]](#)
- Reshak, A.H.; Auluck, S. $\text{LiMoO}_3(\text{IO}_3)_3$, a novel molybdenyl iodate with strong second-order optical nonlinearity. *J. Alloy. Compd.* **2016**, *660*, 32–38. [\[CrossRef\]](#)
- Ngo, N.; Kalachnikova, K.; Assefa, Z.; Haire, R.G.; Sykora, R.E. Synthesis and structure of $\text{In}(\text{IO}_3)_3$ and vibrational spectroscopy of $\text{M}(\text{IO}_3)_3$ ($\text{M} = \text{Al, Ga, In}$). *J. Solid State Chem.* **2006**, *179*, 3824–3830. [\[CrossRef\]](#)
- Pathania, D.; Sharma, G.; Mu, N.; Vishal, P. A biopolymer-based hybrid cation exchanger pectin cerium(IV) iodate: Synthesis, characterization, and analytical applications. *Desalin. Water Treat.* **2016**, *57*, 468–475. [\[CrossRef\]](#)
- Biggs, K.R.; Gomme, R.A.; Graham, J.T.; Ogden, J.S. Characterization of molecular alkali metal iodates by mass spectrometry and matrix isolation IR spectroscopy. *J. Phys. Chem.* **1992**, *96*, 9738–9741. [\[CrossRef\]](#)
- Stahl, K.; Szafranski, M. A neutron powder diffraction study of HIO_3 and DIO_3 . *Acta Cryst. C* **1992**, *48*, 1571–1574. [\[CrossRef\]](#)
- Keve, E.T.; Abrahams, S.C.; Bernstein, J.L. Pyroelectric ammonium iodate, a potential ferroelastic: crystal structure. *J. Chem. Phys.* **1971**, *54*, 2556–2563. [\[CrossRef\]](#)
- Kumar, R.A.; Babu, D.R.; Vizhi, R.E.; Vijayan, N.; Bhagavannarayana, G. Synthesis, growth and optical studies of Mn: $\alpha\text{-LiIO}_3$ single crystal. *Adv. Mater. Res.* **2012**, *584*, 3–7. [\[CrossRef\]](#)
- Bushiri, M.J.; Kochuthresia, T.C.; Vaidyan, V.K.; Gautier-Luneau, I. Raman scattering structural studies of nonlinear optical $\text{M}(\text{IO}_3)_3$ ($\text{M} = \text{Fe, Ga, } \alpha\text{-In}$) and linear optical $\beta\text{-In}(\text{IO}_3)_3$. *J. Nonlin. Opt. Phys. Mater.* **2014**, *23*, 1450039. [\[CrossRef\]](#)
- Mugnier, Y.; Galez, C.; Cretet, J.M.; Bourson, P.; Opagiste, C.; Bouillot, J. Low-frequency relaxation phenomena in $\alpha\text{-LiIO}_3$: The nature and role of defects. *J. Solid State Chem.* **2002**, *168*, 76–84. [\[CrossRef\]](#)
- Kochuthresia, T.C.; Gautier-Luneau, I.; Vaidyan, V.K.; Bushiri, M.J. Raman and FTIR spectral investigations of twinned $\text{M}(\text{IO}_3)_2$ ($\text{M} = \text{Mn, Ni, Co, and Zn}$) crystals. *J. Appl. Spectrosc.* **2016**, *82*, 941–946. [\[CrossRef\]](#)

13. Hermet, P. First-principles based analysis of the piezoelectric response in α -LiIO₃. *Comput. Mater. Science* **2017**, *138*, 199–203.
14. Peter, S.; Pracht, G.; Lange, N.; Lutz, H.D. Zinkiodate-schwingungsspektren (IR, Raman) und kristallstruktur von Zn(IO₃)₂·2H₂O. *Z. Anorg. Allg. Chem.* **2000**, *626*, 208–215. [[CrossRef](#)]
15. Hector, A.L.; Henderson, S.J.; Levason, W.; Webster, M. Hydrothermal synthesis of rare earth iodates from the corresponding periodates: Structures of Sc(IO₃)₃, Y(IO₃)₃·2H₂O, La(IO₃)₃·1/2H₂O and Lu(IO₃)₃·2H₂O. *Z. Anorg. Allg. Chem.* **2002**, *628*, 198–202. [[CrossRef](#)]
16. Bentría, B.; Benbortal, D.; Bagieu-Beucher, M.; Mosset, A.; Zaccaro, J. Crystal engineering strategy for quadratic nonlinear optics. Part II: Hg(IO₃)₂. *Solid State Sci.* **2003**, *5*, 359–365. [[CrossRef](#)]
17. Galez, C.; Mugnier, Y.; Bouillot, J.; Lambert, Y.; le Dantec, R. Synthesis and characterisation of Fe(IO₃)₃ nanosized powder. *J. Alloys Compd.* **2006**, *416*, 261–264. [[CrossRef](#)]
18. Bentría, B.; Benbortal, D.; Hebboul, Z.; Bagieu-Beucher, M.; Mosset, A. Polymorphism of anhydrous cadmium iodate structure of ϵ -Cd(IO₃)₂. *Z. Anorg. Allg. Chem.* **2005**, *631*, 894–901. [[CrossRef](#)]
19. Sun, C.F.; Hu, C.L.; Xu, X.; Ling, J.B.; Hu, T.; Kong, F.; Long, X.F.; Mao, J.G. BaNbO(IO₃)₅: A new polar material with a very large SHG response. *J. Am. Chem. Soc.* **2009**, *131*, 9486–9487. [[CrossRef](#)]
20. Lan, Y.C.; Chen, X.L.; Xie, A.Y.; Jiang, P.Z.; Lin, C.L. Synthesis, thermal and magnetic properties of new metal iodate: (LiFe_{1/3})(IO₃)₂. *J. Cryst. Growth* **2002**, *240*, 526–530. [[CrossRef](#)]
21. Bonacina, L.; Mugnier, Y.; Courvoisier, F.; le Dantec, R.; Extermann, J.; Lambert, Y.; Boutou, V.; Wolf, C.G.J.-P. Polar Fe(IO₃)₃ nanocrystals as local probes for nonlinear microscopy. *Appl. Phys. B* **2007**, *87*, 399–403. [[CrossRef](#)]
22. Taouti, M.B. Synthèses et Caractérisations Structurales D'iodates Métalliques, Matériaux Lasers Convertisseurs de Fréquences. Ph. D. Thesis, Université Joseph-Fourier, Grenoble, France, 2008.
23. Sheng, T.D.; Ming, F.Z.; Xiu, L.W. Investigation of the pseudo-binary system LiIO₃-Zn(IO₃)₂. *Acta Phys. Sin.* **1981**, *30*, 234–241.
24. Kraus, W.; Nolze, G. POWDER CELL: A program for the representation and manipulation of crystal structures and calculation of the resulting X-ray powder patterns. *J. Appl. Cryst.* **1996**, *29*, 301–303. [[CrossRef](#)]
25. Rodriguez-Carvajal, J. Recent advances in magnetic structure determination by neutron powder diffraction. *Physical B* **1993**, *192*, 55–69. [[CrossRef](#)]
26. Garg, A.B.; Errandonea, D. High-pressure powder X-ray diffraction study of EuVO₄. *J. Solid State Chem.* **2015**, *226*, 147–153. [[CrossRef](#)]
27. Caglioti, G.; Paoletti, A.; Ricci, F.P. Choice of collimators for a crystal spectrometer for neutron diffraction. *Nucl. Instrum.* **1958**, *3*, 223–228. [[CrossRef](#)]
28. Liang, J.K.; Wang, C.G. Diffusion of lithium in intercalated compound Li_xTiO₂. *Acta Chim. Sin.* **1982**, *40*, 969–976.
29. Phanon, D.; Bentría, B.; Jeanneau, E.; Benbortal, D.; Mosset, A.; Luneau, I.G. Crystal structure of M(IO₃)₂ metal iodates, twinned by pseudo-merohedry, with MII: MgII, MnII, CoII, NiII and ZnII. *Z. Kristallogr. Cryst. Mater.* **2006**, *221*, 635–642. [[CrossRef](#)]
30. Crettez, J.M.; Coquet, E.; Pannetier, J.; Bouillot, J.; Floch, M.D. Neutron structure refinement of gamma- and beta-lithium: Comparison between alpha, gamma, and beta phases. *J. Solid State Chem.* **1985**, *56*, 133–147. [[CrossRef](#)]
31. Errandonea, D.; Santamaria-Perez, D.; Martinez-Garcia, D.; Gomis, O.; Shukla, R.; Achary, S.N.; Tyagi, A.K.; Popescu, C. Pressure impact on the stability and distortion of the crystal structure of CeScO₃. *Inorg. Chem.* **2017**, *56*, 8363–8371. [[CrossRef](#)]
32. Benmakhlouf, A.; Errandonea, D.; Bouchenafa, M.; Maabed, S.; Bouhemadou, A.; Bentabet, A. New pressure-induced polymorphic transitions of anhydrous magnesium sulfate. *Dalton Trans.* **2017**, *46*, 5058–5068. [[CrossRef](#)] [[PubMed](#)]
33. Freccero, R.; Solokha, P.; Proserpio, D.M.; Saccone, A.; de Negri, S. Lu₅Pd₄Ge₈ and Lu₃Pd₄Ge₄: Two more germanides among polar intermetallics. *Crystals* **2018**, *8*, 205. [[CrossRef](#)]
34. van Troeye, B.; Gillet, Y.; Poncé, S.; Gonze, X. First-principles characterization of the electronic and optical properties of hexagonal LiIO₃. *Opt. Mater.* **2014**, *36*, 1494–1501. [[CrossRef](#)]
35. Clark, S.J.; Segall, M.D.; Pickard, C.J.; Hasnip, P.J.; Probert, M.J.; Refson, K.; Payne, M.C. First principles methods using CASTEP. *Z. Für Krist.* **2005**, *220*, 567–570. [[CrossRef](#)]
36. Perdew, J.P.; Wang, Y. Accurate and simple analytic representation of the electron-gas correlation energy. *Phys. Rev. B* **1992**, *45*, 13244–13249. [[CrossRef](#)] [[PubMed](#)]

37. Lee, D.W.; Kim, S.B.; Ok, K.M. ZnIO₃(OH): A new layered non-centrosymmetric polar iodate–hydrothermal synthesis, crystal structure, and second-harmonic generating (SHG) properties. *Dalton Trans.* **2012**, *41*, 8348–8353. [[CrossRef](#)] [[PubMed](#)]
38. Černý, R. Crystal structures from powder diffraction: Principles, difficulties and progress. *Crystals* **2017**, *7*, 142. [[CrossRef](#)]
39. Gomis, O.; Sans, J.A.; Lacombe-Perales, R.; Errandonea, D.; Meng, Y.; Chervin, J.C.; Polian, A. Complex high-pressure polymorphism of barium tungstate. *Phys. Rev. B* **2012**, *86*, 054121. [[CrossRef](#)]
40. Gomis, O.; Lavina, B.; Rodríguez-Hernández, P.; Muñoz, A.; Errandonea, R.; Errandonea, D.; Bettinelli, M. High-pressure structural, elastic, and thermodynamic properties of zircon-type HoPO₄ and TmPO₄. *J. Phys. Condens. Matter* **2017**, *29*, 095401. [[CrossRef](#)]
41. Toby, B.H. R factors in Rietveld analysis: How good is good enough? *Powder Diffr.* **2006**, *21*, 67–70. [[CrossRef](#)]
42. Errandonea, D.; Kumar, R.S.; Gomis, O.; Manjon, F.J.; Ursaki, V.V.; Tiginyanu, I.M. X-ray diffraction study on pressure-induced phase transformations and the equation of state of ZnGa₂Te₄. *J. Appl. Phys.* **2013**, *114*, 233507. [[CrossRef](#)]
43. Bouillot, J.; Coquet, E.; Pannetier, J.; Cretiez, J.M. Neutron powder diffraction studies of LiIO₃ and (HIO₃, 2LiIO₃). *Physica B + C* **1986**, *136*, 493–497. [[CrossRef](#)]
44. Momma, K.; Izumi, F.J. VESTA: A three-dimensional visualization system for electronic and structural analysis. *Appl. Cryst.* **2011**, *44*, 1272–1276. [[CrossRef](#)]
45. Robinson, K.F.; Gibbs, G.V.; Ribbe, P.H. Quadratic elongation: A quantitative measure of distortion in coordination polyhedral. *Science* **1971**, *172*, 567–570. [[CrossRef](#)] [[PubMed](#)]
46. Liang, J.K.; Rao, G.H.; Zhang, Y.M. Polymorphism phase transition and the relative stability of various phases in the LiIO₃ crystal. *Phys. Rev. B* **1989**, *39*, 459–466. [[CrossRef](#)] [[PubMed](#)]
47. Hu, C.L.; Mao, J.G. Recent advances on second-order NLO materials based on metal iodates. *Coord. Chem. Rev.* **2015**, *288*, 1–17. [[CrossRef](#)]
48. Mugnier, Y.; Galez, C.; Cretiez, J.M.; Bouillot, P.B.J. Dielectric characterization and ionic conductivity of α-LiIO₃ crystals related to the growth conditions. *Sol. State Comm.* **2000**, *115*, 619–623. [[CrossRef](#)]
49. Errandonea, D.; Muñoz, A.; Rodríguez-Hernández, P.; Gomis, O.; Achary, S.N.; Popescu, C.; Patwe, S.J.; Tyagi, A.K. High-pressure crystal structure, lattice vibrations, and band structure of BiSbO₄. *Inorg. Chem.* **2016**, *55*, 4958–4969. [[CrossRef](#)] [[PubMed](#)]
50. Garg, A.B.; Errandonea, D.; Pellicer-Porres, J.; Martinez-Garcia, D.; Kesari, S.; Rao, R.; Popescu, C.; Bettinelli, M. LiCrO₂ under pressure: In-situ structural and vibrational studies. *Crystals* **2019**, *9*, 2. [[CrossRef](#)]
51. Errandonea, D.; Ruiz-Fuertes, J. A brief review of the effects of pressure on wolframite-type oxides. *Crystals* **2018**, *8*, 71. [[CrossRef](#)]
52. Zhang, W.W.; Cui, Q.L.; Pan, Y.W.; Dong, S.S.; Liu, J.; Zou, G.T. High-pressure X-ray diffraction study of LiIO₃ to 75 GPa. *J. Phys. Condens. Matter* **2002**, *14*, 10579–10582. [[CrossRef](#)]
53. Cafferty, M.S. Absorption of LiIO₃ in the infrared for the ordinary direction of propagation. *Infr. Phys. Techn.* **1994**, *35*, 801–804. [[CrossRef](#)]
54. Cretiez, J.M.; Gard, R.; Remoissenet, M. Near and far infrared investigations from α and β lithium iodate crystals. *Solid State Commun.* **1972**, *11*, 951–954. [[CrossRef](#)]
55. Pimenta, M.A.; Oliveira, M.A.S.; Boursond, P.; Cretiez, J.M. Raman study of crystals. *J. Phys. Condens. Matter* **1997**, *9*, 7903–7912. [[CrossRef](#)]
56. Nassau, K.; Shiever, J.W.; Prescott, B.E. Transition metal iodates. I. Preparation and characterization of the 3d iodates. *J. Solid State Chem.* **1973**, *7*, 186–204. [[CrossRef](#)]
57. Cretiez, J.M.; Misset, J.P.; Coquet, E. Vibrations and force constants of the hexagonal lithium iodate crystal. *J. Chem. Phys.* **1979**, *70*, 4194–4198. [[CrossRef](#)]
58. Joulaud, C.; Mugnier, Y.; Djanta, G.; Dubled, M.; Marty, J.C.; Galez, C.; Wolf, J.P.; Bonacina, L.; le Dante, R. Characterization of the nonlinear optical properties of nanocrystals by Hyper Rayleigh scattering. *J. Nanobiotechnol.* **2013**, *11*, S8. [[CrossRef](#)] [[PubMed](#)]

